INT. J. HYPERTHERMIA, 1988, VOL. 4, NO. 5, 497–512

Implantable helical coil microwave antenna for interstitial hyperthermia

TORU SATOH and PAUL R. STAUFFER

Departments of Neurological Surgery and Radiation Oncology, School of Medicine, University of California, San Francisco, CA 94143, U.S.A.

(*Received 31 December 1986; accepted 29 October 1987*)

An implantable helical coil microwave antenna has been developed for improved localization and control of interstitial hyperthermia for deep-seated tumours. A helical coil structure was employed as an extension of the inner conductor at the terminal portion of a miniature semi-rigid coaxial cable. The antennas were constructed with three different connection configurations of the helical coil to the feedline, and with several coil turn densities during the optimization of heating characteristics. In order to compare relative antenna heating performance, a set of quantitative parameters was introduced. Power deposition profiles of 2450 MHz helical coil antennas were studied in both phantom models and muscle tissue *in vivo*, and compared to those of commonly used dipole antennas. Optimal antenna performance was obtained with a 10-turn per 1 cm helical coil connected to the inner conductor at the tip and separated from the outer conductor by a 0·1 cm gap (HCS-10). These antennas produced a well-localized heating pattern with a sharp falloff of temperature in both directions axially from the coil element. For half-wavelength insertion depths, the effective heating length (50 per cent of maximum SAR) of HCS-10 antennas matched that of standard dipole antennas, but was shifted down towards the tip. For shorter and deeper antenna insertion depths the HCS-10 heating pattern remained similarly localized to the region surrounding the helical coil with minimal cold zone at the tip. In contrast, the dipole antenna heating pattern changed significantly depending on insertion depth, with an unavoidable 0·2–0·7 cm cold region at the antenna tip and elevated surface temperatures for short insertion depths.

Key words: hyperthermia, interstitial hyperthermia, microwave antenna, thermal dosimetry.

1. Introduction

In order to deliver effective hyperthermia treatments in deep-seated critical vascular or neural tissues it is essential to control the size and location of the induced thermal field accurately. Interstitial hyperthermia appears to offer the best chance of both penetration and localization of the thermal field to a specific volume at depth. There are presently three interstitial heating techniques: radiofrequency current field (Astrahan and Norman 1982, Vora *et al.* 1982), microwave (Strohbehn *et al.* 1979, King *et al.* 1983, Samaras 1984, Trembly 1985, Neyzari and Cheung 1985), and inductively heated ferromagnetic seeds (Stauffer *et al.* 1984 a, Brezovich *et al.* 1984). In its current form, radiofrequency interstitial heating appears less suitable for heating of critical tissue regions such as brain, because of difficulties in the management of indwelling metal electrodes. Ferromagnetic seed heating awaits refinements in the thermoregulating seed alloys and implant techniques, and commercialization of the equipment.

Correspondence should be addressed to Paul R. Stauffer, M.S.E.E., Hyperthermia Section of the Department of Radiation Oncology, Box 0226, University of California at San Francisco, San Francisco, CA 94143, U.S.A.

To date, only microwave antennas have been used for clinical interstitial hyperthermia treatment of intracranial neoplasms (Salcman and Samaras 1981, Winter *et al.* 1985, Roberts *et al.* 1986). This is primarily because the antennas can be placed in the same plastic catheters as are used for the brachytherapy sources. Additionally, microwave antennas have the capability of deeper heating field penetration into surrounding tissues near mid-depth of the antennas over other interstitial techniques, which can result in a reduction of the required implant density within the treatment volume (Mechling and Strohbehn, 1986).

Nevertheless, there are several problems with standard dipole microwave antennas which restrict the applicability of interstitial microwave hyperthermia (de Sieyes *et al.* 1981, Emami and Perez 1985, Sneed *et al.* 1986). Because the operating frequency and dipole dimensions are major determinants of the radiated field, there is little flexibility in choosing the antenna length and total insertion depth in tissue to coincide with specific tumour dimensions. If suboptimal combinations of dipole length and implant depth are attempted, overheating of tissue at the antenna entrance site or otherwise unsuitable heating patterns can result. Even with half-wavelength insertions, actual temperature distributions along the antenna length are gaussian-shaped with a prominent peak adjacent to the outer conductor discontinuity (gap) and a dramatic falloff of temperature in either direction axially from the gap. Tissue near the tip of such antennas is often not heated effectively, so that significant over-implanting of the deep aspect of the tumour volume is required.

To minimize the effect of these problems, and to facilitate heating a larger variety of tumours and tumour sites, especially those located in critical neural or vascular tissues, a new antenna is required which can restrict the thermal field to the desired location independently of insertion depth with effective heating extended out to the antenna tip. We have developed such an antenna in which we employed a variable-length spiral-wound 'helical coil' as an extension of the coaxial feedline inner conductor. By changing the turn density and connection configuration of the coil, it was possible to alter the antenna heating pattern to the most desirable shape. In the present study the power deposition profiles of three different helical coil antenna configurations were compared at 2450 MHz to the performance of an interstitial dipole antenna. Extensive comparative studies in phantom models were followed by a verification of the results in canine thigh muscle tissue *in vivo*.

2. Materials and methods

2.1. *Antenna design*

Five different antenna configurations (figure 1) were constructed for this study from 0·095 cm OD semi-rigid coaxial cable (Uniform Tubes, Inc., Collegeville, PA). Type I (Dipole-Bare End, DB) antennas (de Sieyes *et al.* 1981) were constructed by stripping off the outer conductor of the coaxial cable for a distance of 1·1 cm (approximately quarter wavelength in catheter/tissue load at 2450 MHz) from the tip and cutting away 0·1 cm of the inner conductor insulation at the tip. Type II (Dipole-Regular, DR) antennas (Samaras 1984, Sneed *et al.* 1986) were constructed by cutting a 0·1 cm break (gap) in the outer conductor at a distance of 1·1 cm from the tip. The distal 1·0 cm length of the outer conductor was electrically connected as an extension of the inner conductor by soldering at the tip. Type II antennas were also constructed with a smaller diameter 0·058 cm OD coaxial cable (Dipole-Thin, DT). While these 'dipole'-like antenna designs differ theoretically from several dipole antennas reported in the literature (Taylor 1978, Strohbehn *et al.* 1979, Lyons *et al.* 1984, Trembly 1985), previous dosimetry experience in our laboratory has shown that essentially identical

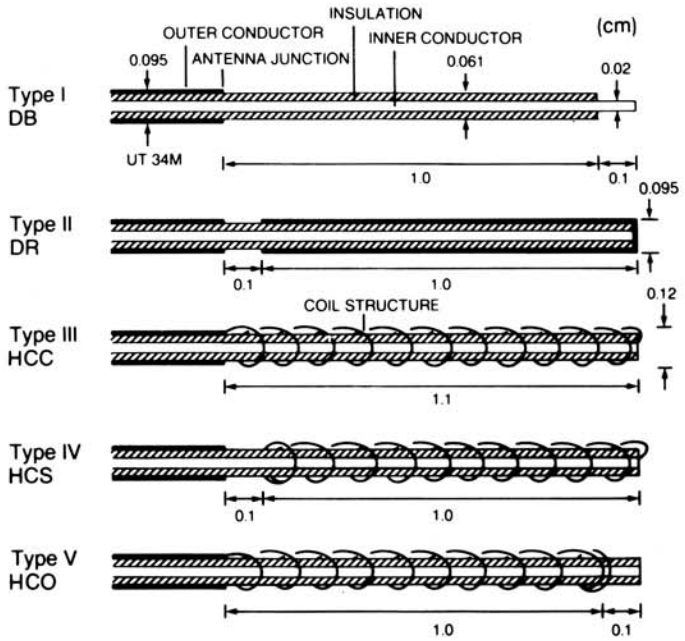

Figure 1. Schematic illustration of the implantable microwave antenna configurations tested in this work: dipole-bare end (DB, Type I), dipole-regular (DR, Type II), helical coil-connected (HCC, Type III), helical coil-separated (HCS, Type IV), and helical coil-open end (HCO, Type V) microwave antennas.

heating patterns are obtained with both antenna styles.

Types III, IV, and V antennas were functional variations of a new antenna style based on a helical coil conductor extension of the antenna feedline. Coils for each antenna were constructed by wrapping wire tightly around a stainless steel wire-form using three different turn densities: 7, 10, and 16 turns per 1 cm length. After extracting the wire form the helical coils were installed over the 0·061 cm OD bare dielectric coating of the coaxial cable inner conductor. Several wire types were investigated, including 0·02 cm OD silver-plated copper wire (SPCW), 0·02 cm OD polyethylene-coated copper wire, and 0·032 cm OD nichrome wire. Type III antennas consisted of a helical coil-connected (HCC) configuration in which the helical coil was used as a direct connection between the inner and outer conductors of a dipole-bare antenna by soldering the coil at both ends. Three variations of HCC antennas were made according to the number of coil turns: HCC-7/10, HCC-10/10, and HCC-16/10. Type IV helical coil-separated (HCS) antennas were constructed with the coil soldered to the inner conductor at the tip but left separated from the end of the outer conductor by a 0·1 cm gap. Three variations were made: HCS-7/10, HCS-10/10, and HCS-16/10. Type V helical coil-open end (HCO) antennas were constructed with 10- and 16-turn coils soldered to the coax outer conductor only: HCO-10/10 and HCO-16/10. All antennas fit inside 16-gauge (0·122 cm ID) Teflon catheters. A thermal conduction heater with dimensions similar to the antennas described above was made by inserting a 0·058 cm OD copper tube (water inlet) into a closed-end 19-gauge (0·1 cm ID) plastic catheter (water outlet) and circulating hot water through the closed circuit. This self-contained hot water heater also fits inside the 16-gauge catheter for direct comparison with the microwave antenna heating performance.

2.2. *Phantom models*

Tissue equivalent brain phantoms of two different TX-150 based compositions (Chou *et al.* 1984) were used during the *in vitro* antenna optimization and testing period. The material was contained in an 8 × 8 × 11 cm Plexiglas box traversed by an array of 16-gauge Teflon catheters in a 0·5 cm grid for holding antennas and multi-sensor temperature probes. Six phantom models were constructed during the course of the study to reduce the errors from phantom mixture and catheter spacing variations. The reproducibility of power deposition profiles in the different phantom models was assessed using reference antennas of DR and HCS-10 construction for standardized tests in each new phantom.

2.3. *General experimental procedures*

For all tests, antennas were driven at 2450 MHz using a continuous wave microwave power source (Model CA2450, Cheung Lab. Inc., Lanham-Seabrook, MD). Power fed to each antenna was tuned with a double stub tuner (Model 1729, Maury Microwave, Cucamonga, CA) for optimum impedance match to the generator, since no attempt was made to trim each antenna to exactly 50 ohms. Although the antennas were adequately matched alone (typical return loss of about −8 dB or VSWR ≃ 2·3), precise and reproducible matching of the antennas to the source frequency and phantom load was accomplished using the tuners (figure 2). The power required to elevate the temperature of the surrounding phantom approximately 2–3°C max in 30 s varied between 3 and 5 W. A multiple-sensor optical fibre probe (Clini-Therm Corp., Dallas, TX) with four sensors spaced 0·25 cm apart was inserted in a catheter parallel to and 0·5 cm away from the antenna axis, for measuring the temperature. Using a separate stationary single sensor temperature probe located mid-depth in a second

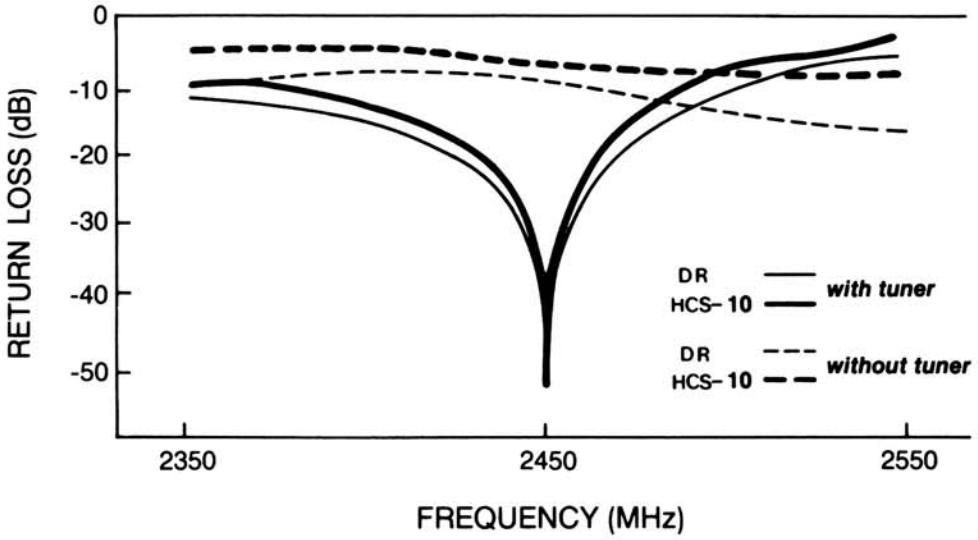

Figure 2. Impedance characteristic of typical DR and HCS-10 antennas inserted 2·1 cm in 16-gauge Teflon catheter in phantom material with and without a double-stub tuner. Without the tuner, both antenna styles show a broadband weakly matched condition with a return loss of − 9 dB (VSWR = 2·1) for the DR and a return loss of − 7·5 dB (VSWR = 2·4) for the HCS-10 antennas at 2450 MHz. Using the tuner, optimal matching conditions could be obtained for both antennas at the desired microwave frequency of 2450 MHz (return loss = − 50 dB, VSWR = 1·006).

parallel ($r = 0{\cdot}5$ cm) catheter as control between trials, longer axial profiles were measured by moving the multi-sensor probe 1 cm and repeating the heat trial after cool-down of the phantom to initial conditions. Thus, multiple 30 s heat trials were performed in order to piece together the power deposition profile of each antenna configuration.

2.4. *Power deposition studies*

In order to compare the axial power deposition profiles of different antenna configurations, single antennas were sequentially inserted 2·1 cm into the same catheter of the phantom so that the outer conductor gap was 1·0–1·1 cm below the phantom surface. Studies were performed to investigate the effect of varying connection configuration of the helical coil to the inner and/or outer conductors of the coax cable. Thus, HCC, HCS and HCO antennas were compared using the same 10 turns per 1·0 cm length helical coil and feedline assembly. Effects of antenna insertion depth on the axial profiles were evaluated with DR and HCS-10 antennas using insertion depths of 1·35 and 3·1 cm, as well as the standard 2·1 cm, phantom surface to the antenna tip distance.

Power deposition profiles in the radial direction were investigated in the plane of the antenna gap for both DR and HCS-10 antennas with insertion depths of 2·1 cm, and were compared to the temperature falloff from a hot (90°C) water circuit inserted in the same 16-gauge Teflon catheters in phantom as a control for strictly thermal conduction heating.

2.5. In vivo *experiments*

In order to verify the relevance of the comparative power deposition study in phantom, the power deposition profiles from DR and HCS-10 antennas were compared in relatively homogeneous and well-perfused normal canine thigh muscle tissue *in vivo*. A method involving repeated heating experiments in the same implant site (Stauffer *et al.* 1986) was used for a direct comparison of profiles induced by the two antennas with three different insertion depths (2·1, 3·1, and 4·1 cm from the skin surface to antenna tip).

Experiments were performed in 14 implant sites in seven dogs. Each dog was premedicated with atropine sulphate and acepromazine, and was maintained at a surgical level of anaesthesia with methoxyflurane and oxygen. A row of three parallel 14-gauge trocars was inserted through skin and 4 cm of thigh muscle tissue, using a 2 cm thick Plexiglas template with a 0·5 cm grid. A fourth lateral trocar was placed perpendicular to and touching the first three, through an attached template. Closed-end 16-gauge Teflon catheters with steel stylets were inserted and all trocars withdrawn. A single antenna was placed in the central catheter of the row. A multi-sensor probe with four sensors spaced 1 cm apart, and a single sensor probe, were inserted through catheters at each side parallel to and 0·5 cm away from the antenna. After mapping the initial temperature distribution *in vivo*, 2450 MHz microwave power was applied to obtain steady-state temperature conditions within approximately 10 min. The temperature distribution was recorded in the following 5–10 min by mapping the multi-sensor probe in 0·2 cm increments along the catheter. The stationary single sensor probe was used for feedback temperature control during the trial and between subsequent trials. Power was adjusted manually to maintain a temperature of $43{\cdot}0 \pm 0{\cdot}2$°C at the control site. Comparative trials with other antennas followed a 30 min break to allow the tissue to return to initial temperature conditions. The order of antenna trials was varied in the different implant sites and the results averaged to minimize the effect of antenna test sequence.

2.6. *Data analysis and quantitiative parameters*

The power deposition profile of each antenna was determined by repetitive tests in multiple phantom models using more than one antenna of each configuration. The data from corresponding trials were averaged together by first normalizing the SAR (specific absorption rate) of each measured point to the maximum SAR of each linear distribution (normalized SAR profile), and then averaging the normalized profiles together. This analysis was used to allow appropriate averaging of many independent SAR profiles which had varying absolute peak SAR's due to minor differences in input power, heating time, catheter spacing, and probe positioning during the various heat trials.

Since the parameter of interest for this study was the relative heating characteristics of two different antennas and not the absolute temperature distribution or toxicity of a specific tissue site, the *in vivo* steady-state temperature distributions were expressed as temperature differentials above baseline (delta-T). Furthermore, in order to average and compare distributions obtained in different animal implant sites with varying initial temperature conditions, the delta-T profiles were each normalized to a percentage of the peak delta-T of the profile and plotted as percentage delta-temperature.

Several parameters derived from the $r = 0{\cdot}5$ cm axial profiles were used to quantify antenna heating effectiveness, as shown in figure 3: (1) uniformity of power deposition as determined by the length of tissue in cm exhibiting greater than 50 per cent of the maximum tissue temperature rise or SAR (50 per cent heating length, 50 per cent HL); (2) location of the heating peak relative to the phantom surface (peak depth); (3) ability to localize heat only in a desired region along the antenna axis as described by the steepness of the power deposition gradient with depth (percentage squareness);

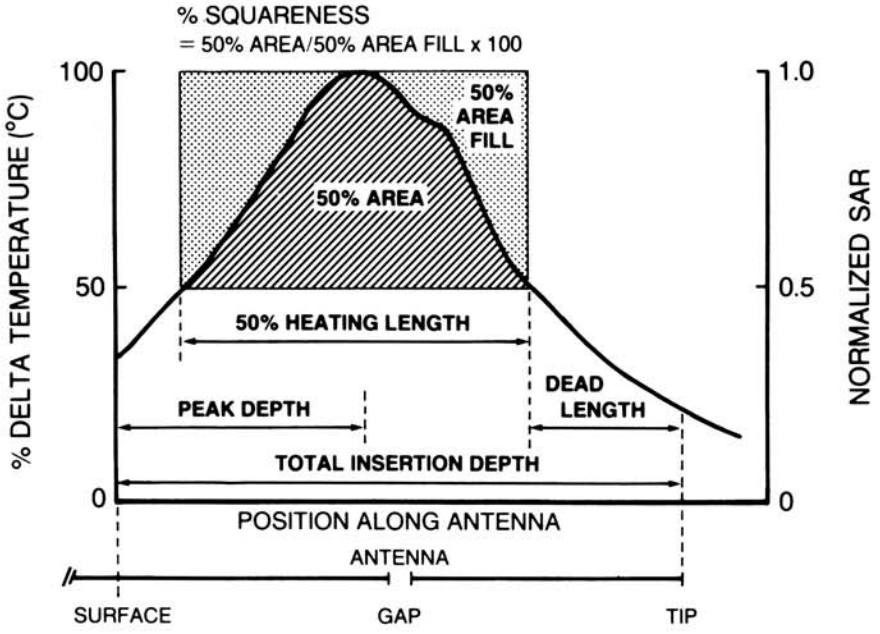

Figure 3. Schema showing the parameters used for the comparative evaluation of $r = 0{\cdot}5$ cm axial power deposition profiles: including the location of the profile temperature peak (normalized-SAR_{max}) with respect to the surface (peak depth), effective heating length ≥ 50 per cent of the normalized-SAR_{max} (50 per cent HL), ability to localize heat—calculated by 50 per cent area/50 per cent area fill (percentage squareness), and axial length at the antenna tip ≤ 50 per cent normalized-SAR_{max} (dead length).

(4) length of tissue near the antenna tip which showed less than 50 per cent of the minimum temperature rise or SAR (dead length); and (5) radial penetration depth as determined via the expression:

$$T(r) = A \,.\, \exp(B \,.\, r) \tag{1}$$

where A was an amplitude constant, B was the exponential rate constant, and r was the radial distance from the antenna surfaces in the plane of the antenna 'gap'. From eqn. (1), the exponential rate constant was calculated and heating field penetration radially away from the antenna was estimated as the depth into tissue exhibiting $\geqslant 50$ per cent of the maximum temperature rise or SAR (50 per cent penetration depth, 50 per cent PD).

3. Results

3.1. *Power deposition profiles in phantom*

Data quantifying the axial ($r = 0{\cdot}5$ cm) profiles for each antenna configuration in phantom are summarized in table 1. The power deposition characteristics of DR antennas were found to be essentially identical in shape to those of both dipole-bare end and dipole-thin antennas (figure 4). For all three antennas, the distribution peak was just proximal to the gap, 0·75 cm from the phantom surface. The profiles exhibited a sloping shoulder extending the effective 50 per cent HL to approximately 1·32–1·44 cm in length. All dipole antennas failed to heat tissue effectively near the antenna tip with dead lengths ranging from 0·48 to 0·60 cm of the 2·1 cm total inserted length.

The power deposition patterns of the Type III (HCC) and Type V (HCO) antenna configurations varied strongly dependent on the helical coil turn density. HCC-7 and HCO-16 antennas showed profiles similar to those of the DR antennas. HCC-10, HCC-16, and HCO-10 antennas showed potentially improved heating patterns with a slightly longer 50 per cent HL and decreased dead lengths. Type IV (HCS) antennas also produced variable heating characteristics according to the turn density of the helical coil. With a near-optimum 10 turns per 1 cm length, however, the HCS-10

Table 1. Axial power deposition profiles in phantom material.

Type	Antenna	No. of tests	Insertion depth (cm)	Peak depth (cm)	50 per cent HL (cm)	Squareness (%)	Dead length (cm)
I	DB	8	2·1	0·65	1·36	55·8	0·56
II	DR	24	2·1	0·75	1·44	61·3	0·48
	DT	8	2·1	0·75	1·32	57·5	0·60
III	HCC-7	8	2·1	0·75	1·34	62·3	0·52
	HCC-10	12	2·1	1·25	1·55	60·9	0·26
	HCC-16	4	2·1	1·25	1·82	48·0	0·00
IV	HCS-7	8	2·1	0·75	1·43	50·2	0·50
	HCS-10	20	2·1	1·50	1·25	56·3	−0·07
	HCS-16	16	2·1	1·25	1·40	61·5	0·19
V	HCO-10	8	2·1	1·25	1·66	60·9	0·13
	HCO-16	4	2·1	1·25	1·35	55·2	0·32

Comparative parameters defined in figure 3 and section 2.6. All helical coils were constructed of 0·032 cm OD nichrome wire. Negative values of dead length represent an extension of the 50 per cent heating length beyond the antenna tip.

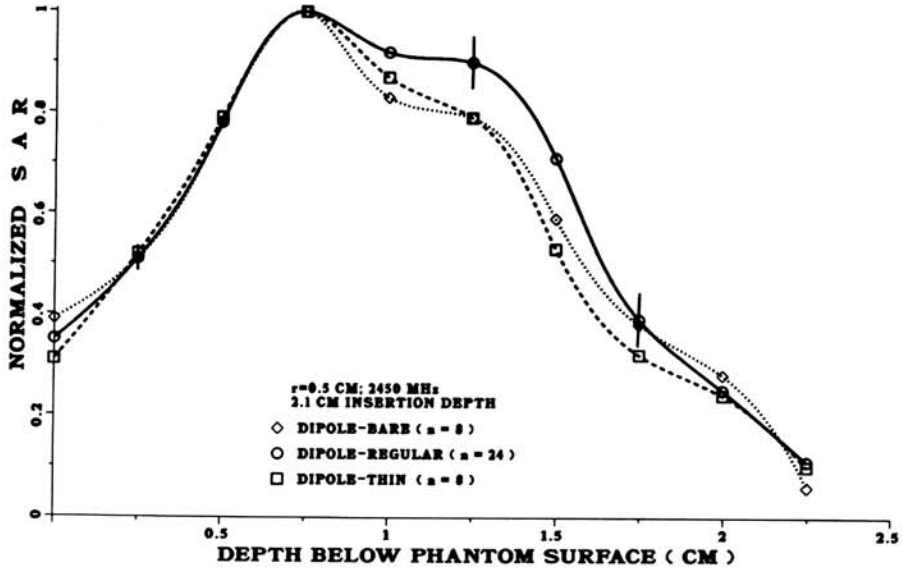

Figure 4. Axial ($r = 0{\cdot}5$ cm) power deposition (SAR) profiles of dipole-bare end (DB), dipole-regular (DR), and dipole-thin (DT) antennas inserted 2·1 cm into 2450 MHz phantom material. Profiles parallel to and 0·5 cm away from the antenna axis are shown as normalized-SAR—calculated from the increase of temperature above baseline (delta-T) after 30 s heating. The average maximum SAR values were $54{\cdot}3 \pm 9{\cdot}1$ W/kg/W input power for DB, $71{\cdot}5 \pm 4{\cdot}9$ W/kg/W for DR, and $59{\cdot}1 \pm 4{\cdot}8$ W/kg/W for DT. The vertical bars represent standard deviation of the mean (SD) for the number (n) of independent phantom trials.

antenna was most effective at localizing the heating to the region surrounding the implanted helical coil by producing a 1·25 cm long 50 per cent HL which extended approximately 0·1 cm past the coil in both directions axially and was centred at the mid-coil depth of 1·5 cm for 2·1 cm insertion depth tests (figure 5). The HCS-10 antenna configuration showed the most prominent localization and shifting of the effectively heated region toward the antenna tip, while the HCC-10 and HCO-10 antennas produced a broader almost double peaked heating pattern (figure 6).

Comparative radial profiles at mid-depth for DR and HCS-10 antennas and thermal conduction heaters are shown in figure 7. The exponential rate constant as determined from the 30 s temperature rise data at distances of $r = 0{\cdot}08$, 0·22, 0·45, 0·69, and 0·93 cm from the heat sources was $-4{\cdot}00 \pm 0{\cdot}32$ for the HCS-10 antenna, $-3{\cdot}14 \pm 0{\cdot}56$ for the DR antenna, and $-6{\cdot}92 \pm 0{\cdot}39$ for the simple thermal conduction heater. The effective 50 per cent penetration depths of the DR, HCS-10, and heated water circuits were calculated to be 0·31, 0·24 and 0·19 cm, respectively (see table 3).

Studies of the reproducibility of the power deposition profiles from DR and HCS-10 antennas tested in phantoms I through VI disclosed no significant variation in the location of peak depth, 50 per cent HL, or dead length, and only a small (< 10 per cent) difference in the percentage squareness parameter.

3.2. *Effects of insertion depth*

The axial ($r = 0{\cdot}5$ cm) power deposition pattern of DR antennas was strongly dependent on insertion depth. With a 3·1 cm insertion, the depth profile was almost

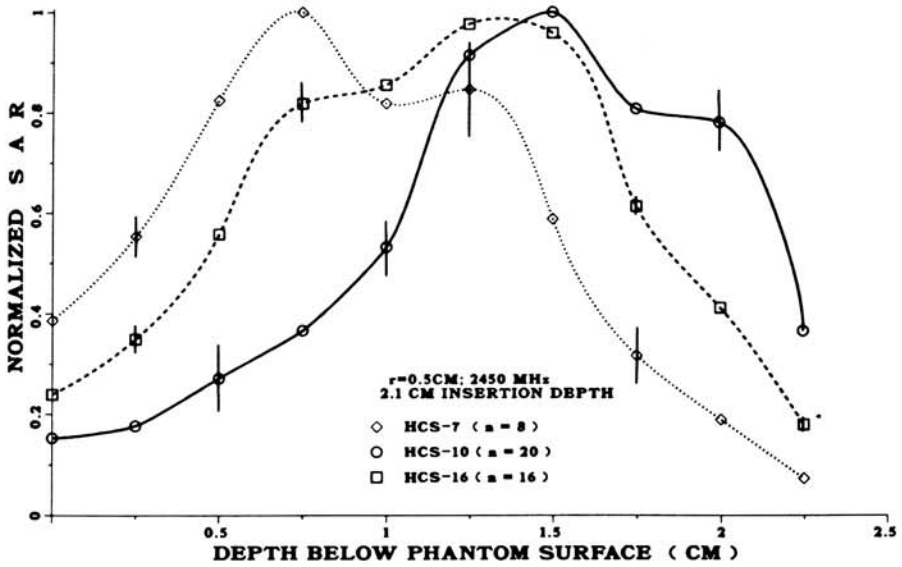

Figure 5. Axial ($r = 0{\cdot}5$ cm) SAR profiles of helical coil-separated (HCS) antennas with three different turn density coils as 7, 10, and 16 turns per 1 cm length (HCS-7, HCS-10, and HCS-16). Antennas were placed in phantom models with a total insertion depth of 2·1 cm and driven at 2450 MHz. The average maximum SAR values were $78{\cdot}2 \pm 4{\cdot}0$ W/kg/W for HCS-7, $60{\cdot}7 \pm 7{\cdot}2$ W/kg/W for HCS-10, and $70{\cdot}0 \pm 6{\cdot}6$ W/kg/W for HCS-16. Vertical bars represent the SD of n trials.

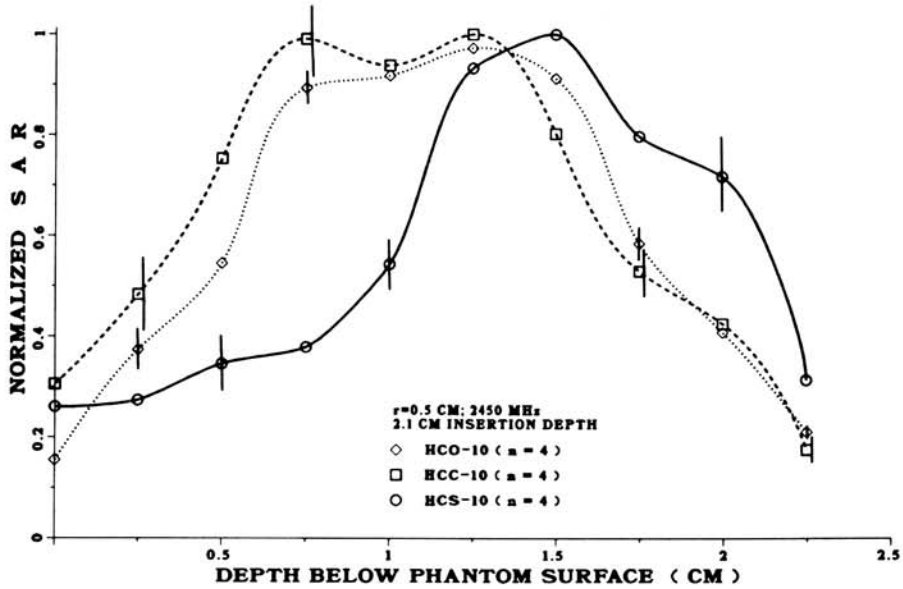

Figure 6. Axial ($r = 0{\cdot}5$ cm) SAR profiles in 2450 MHz phantom of helical coil antennas with three different coil connection configurations; helical coil-connected (HCC-10), helical coil-separated (HCS-10), and helical coil-open end (HCO-10). All antennas used the same helical coil section with 10 turns per 1 cm length. Vertical bars represent the SD of n trials.

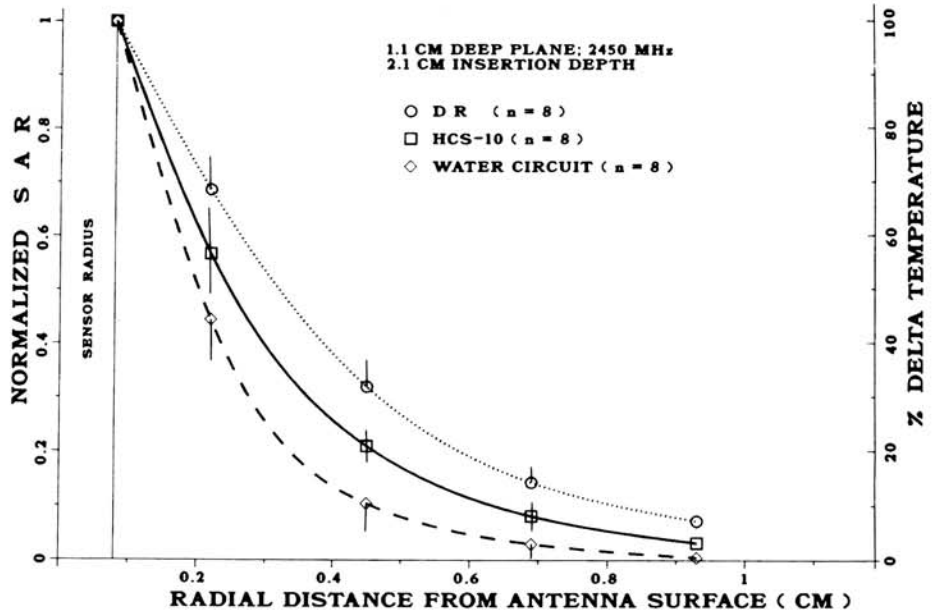

Figure 7. Radial SAR profiles at $t = 30$ s for DR and HCS-10 antennas compared to the temperature falloff from a heated water circuit of equivalent size. The radial profiles were obtained in the plane of the antenna outer conductor gap at a depth of 1 cm from the phantom surface. Vertical bars represent the SD of n independent trials.

symmetric with the peak located 1·5 cm below the surface and a 50 per cent HL and dead length of 2·04 and 0·68 cm, respectively (figure 8a). For shallow insertion depths of 1·35 cm (gap depth of 0·25 cm), the dead length was reduced to 0·17 cm and the 50 per cent HL was 1·21 cm, but the antenna entrance point was overheated with 78 per cent of the peak SAR exhibited near the surface. In contrast, the profiles of HCS-10 antennas were almost identical regardless of insertion depth. The temperature peak moved correspondingly deeper with increasing insertion depth, remaining 0·5 cm proximal to the antenna tip, midway along the helical coil for all tests (figure 8b). The 50 per cent HL for 1·35, 2·1, and 3·1 cm insertion depths was a constant 1·2 cm and the dead length remained essentially zero. Differences in the power deposition profiles were quantified in table 2.

3.3. In vivo *trials*

In general, the HCS-10 antennas produced a broad temperature peak and plateau region along the helical coil length with a sharp dropoff both towards the surface and just past the antenna tip in dog thigh muscle (figure 9a). The profiles revealed effective localization of the heated region around the coil element which was independent of antenna insertion depth. In contrast, the profile from dipole antennas fell off sharply from the peak towards the antenna tip, but tailed off gradually towards the surface, sometimes producing excessive temperatures near the antenna entrance point. Moreover, the profiles were strongly dependent upon insertion depth and failed to heat tissue out to the antenna tip (figure 9b). For insertion depths of 2·1 cm, the temperature profiles of the two antennas were quite different with peak depths of 0·9 cm for the DR antenna and 1·5 cm for the HCS-10 antenna; both had 1·9 cm 50 per cent HL values. When implanted 3·1 cm, the DR 50 per cent HL increased to 2·9 cm while the HCS-10

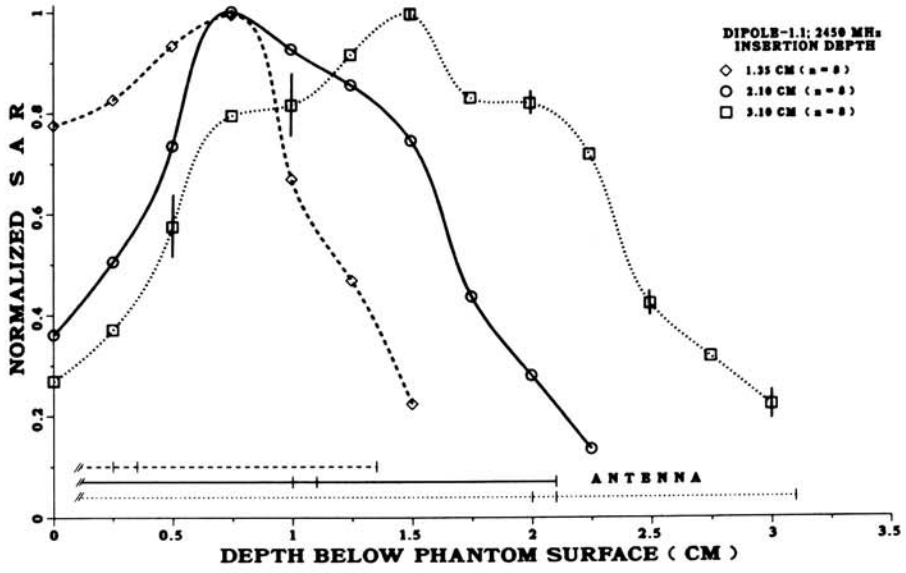

(*a*)

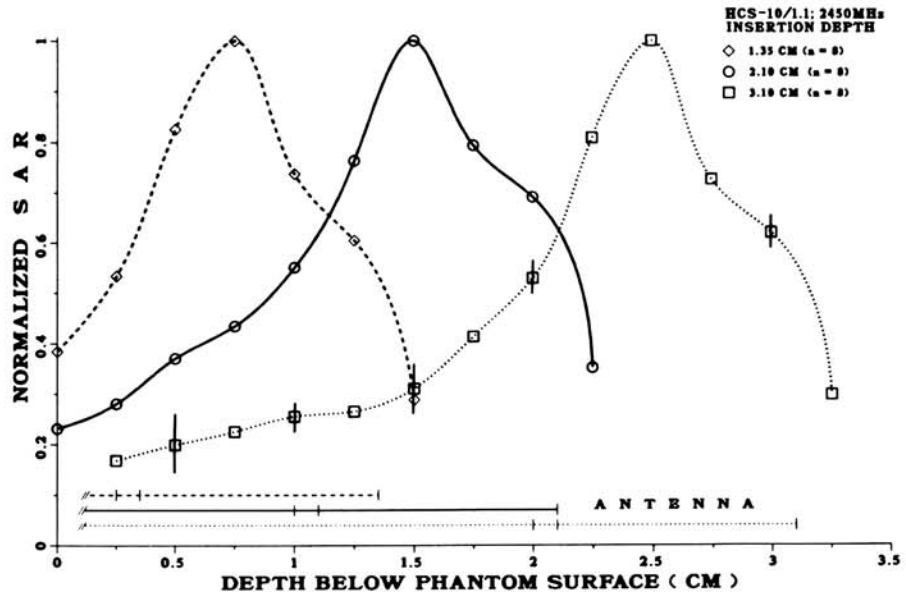

(*b*)

Figure 8. (*a*) Axial ($r = 0{\cdot}5$ cm) SAR profiles of 2450 MHz dipole-regular (DR) antennas with total insertion depths of 1·35, 2·1, and 3·1 cm in phantom models. Compare distributions with those of figure 8b, which were obtained in the same phantom sites using identical trial conditions. Vertical bars represent the SD of n trials. (*b*) Axial ($r = 0{\cdot}5$ cm) SAR profiles of 2450 MHz HCS-10 antennas with total insertion depths of 1·35, 2·1, and 3·1 cm in phantom models. Note the relative independence of heating patterns with insertion depth as compared to figure 8a dipole antennas. Vertical bars represent the SD of n trials.

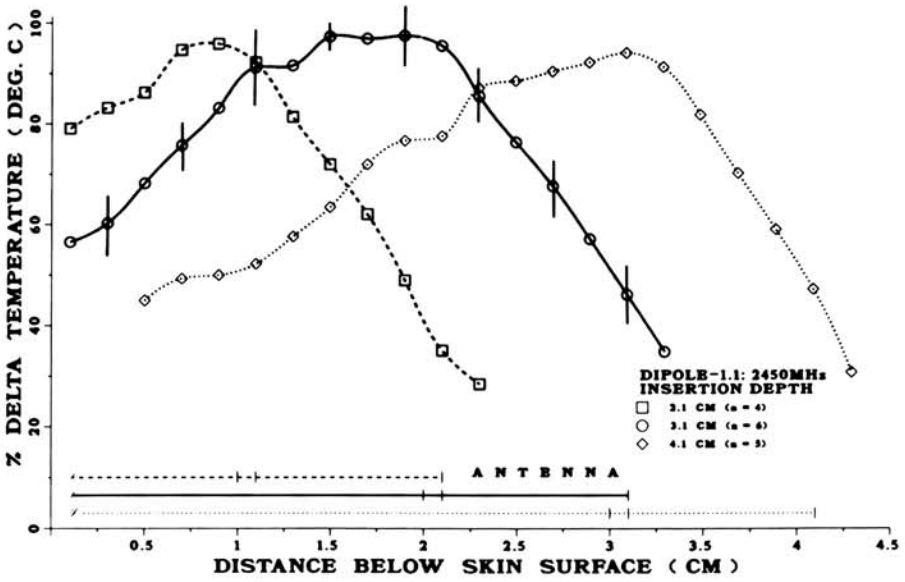

(*a*)

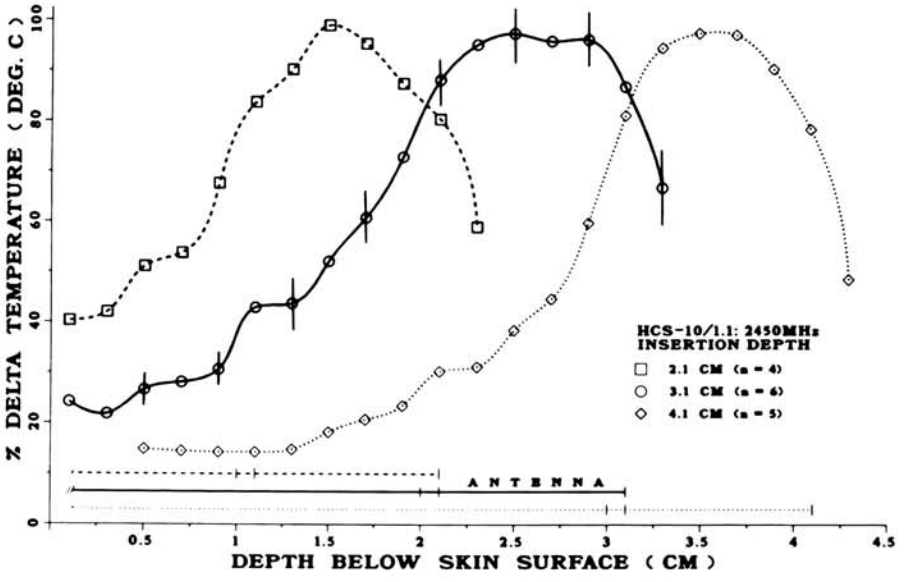

(*b*)

Figure 9. (*a*) Comparative axial ($r = 0{\cdot}5$ cm) thermal profiles of DR antennas with 2·1, 3·1, and 4·1 cm total antenna insertion depths in dog thigh muscle tissue *in vivo*. A procedure involving repeated heating experiments in the same implant site was used for the direct comparison of profiles of the DR and HCS-10 (figure 9b) antennas. The vertical bars represent the SD of n different *in vivo* trials. (*b*) Comparative axial ($r = 0{\cdot}5$ cm) thermal profiles of HCS-10 antennas with 2·1, 3·1, and 4·1 cm total insertion depths in dog thigh muscle tissue *in vivo*. Note the effective localization of heating at depth and similarity of heating patterns regardless of implant depth. Vertical bars represent the SD for n implant sites.

Table 2. Effects of insertion depth on axial power deposition profiles.

Antenna	No. of tests	Insertion depth (cm)	Peak depth (cm)	50 per cent HL (cm)	Squareness (%)	Dead length (cm)
DR	8	1·35	0·75	1·21	62·6	0·17
	8	2·10	0·75	1·45	59·0	0·45
	8	3·10	1·50	2·04	58·9	0·68
HCS-10	8	1·35	0·75	1·19	50·0	0·00
	8	2·10	1·50	1·24	52·1	0·04
	8	3·10	2·50	1·22	49·2	−0·02

Comparative parameters defined in figure 3 and section 2.6. All helical coils were constructed of 0·032 cm OD nichrome wire. Negative values of dead length represent an extension of the 50 per cent heating length beyond the antenna tip.

antenna remained at 1·9 cm. Similarly for 4·1 cm insertion in muscle, the HCS-10 antennas produced the same well-localized heating pattern out to the antenna tip while the DR antenna heating pattern broadened again to a 50 per cent HL of 3·3 cm.

Exponential rate constants determined from the mid-depth radial temperature gradients of DR, HCS-10, and thermal conduction only heaters were calculated as $-0{\cdot}86 \pm 0{\cdot}29$, $-1{\cdot}17 \pm 0{\cdot}60$, and $-1{\cdot}90 \pm 0{\cdot}31$, respectively (table 3). The 50 per cent PDs were estimated to be 0·94 cm for DR and 0·73 cm for HCS-10 antennas, and 0·47 cm for the conductive heaters. The steady-state radial temperature distributions measured 1 cm from the end of 3·1 cm deep heaters were shown in figure 10.

4. Discussion

There is considerable biological and clinical rationale for the use of hyperthermia in the treatment of malignant tumours (Hahn 1979, Dewey 1984, Moorthy *et al.* 1984, Perez and Emami 1985). Direct treatment of the tumour via interstitial hyperthermia appears to increase the potential for uniform heating of the tumour volume while sparing surrounding tissues. Of the three interstitial heating techniques (Strohbehn *et al.* 1979, Vora *et al.* 1982, Stauffer *et al.* 1984 b), invasive microwave antennas are currently the logical choice for adjuvant use with brachytherapy (Gutin *et al.* 1984, Hall 1985) due to the similarity of surgical considerations such as implant catheter size and placement.

Table 3. Relative radial heat penetration depths in phantom material and muscle tissue.

	Phantom material			Muscle tissue		
Antenna	No. of tests	Exponential constant	50 per cent PD (cm)	No. of tests	Exponential constant	50 per cent PD (cm)
DR	8	$-3{\cdot}14 \pm 0{\cdot}56$	0·31	8	$-0{\cdot}86 \pm 0{\cdot}29$	0·94
HCS-10	8	$-4{\cdot}00 \pm 0{\cdot}32$	0·24	8	$-1{\cdot}17 \pm 0{\cdot}60$	0·73
Heater†	8	$-6{\cdot}92 \pm 0{\cdot}39$	0·19	6	$-1{\cdot}90 \pm 0{\cdot}31$	0·47

Comparative parameters defined in section 2.6 of text. Data were obtained with 2·1 cm insertion depth in phantom material and 3·1 cm insertion depth in muscle tissue.

†Heated water circuit placed inside same 16-gauge Teflon catheter as antennas.

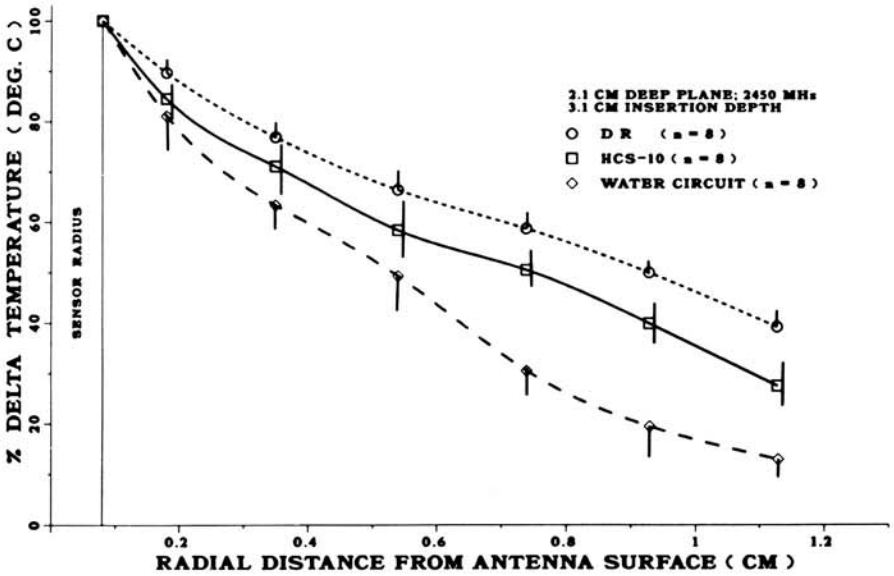

Figure 10. Comparative radial thermal profiles of DR and HCS-10 antennas with thermal conduction only heating in dog thigh muscle tissue *in vivo*. Profiles measured 2·1 cm from the surface in the plane of the antenna gaps, with a total antenna insertion depth of 3·1 cm. Vertical bars represent the SD for *n* implant sites.

There have been many reports of both theoretical and experimental studies of dipole microwave antennas for interstitial hyperthermia (Taylor 1978, Strohbehn *et al.* 1979, de Sieyes *et al.* 1981, Samaras 1984, King *et al.* 1983, Trembly 1985, Sneed *et al.* 1986). Most of the reports describe the axial direction thermal profiles of antennas implanted about a half-wavelength in tissue, while ignoring the different insertion depths which might more accurately model many intended treatment situations. Little information is available on the actual heating patterns obtained with non-optimal insertion depths, nor on the radial depth distributions at points along the antenna other than through the central 'gap' or 'junction' plane.

For the present study we developed a helical coil microwave antenna configuration which can improve the heating field localization at depth in tissue. The heating pattern, which extends out to the antenna tip, was shown to be desirable for heating critical neural or vascular tissues where over-implanting of the tumour volume is not acceptable. Comparative thermal dosimetry results indicated that the heating profiles of HCS-10 antennas showed significant improvement over simple dipole antenna configurations in terms of insertion depth independent heating, more uniform heating along the antenna axis, and effective antenna tip heating.

Although there was little difference between the two antennas in 50 per cent HL and percentage squareness parameters for the 2·1 cm insertion depth, the dipole antenna parameters varied with changing implant conditions while the helical coil parameters remained essentially constant. While the radial temperature falloff of dipole antennas showed slightly deeper penetration in the plane of the outer conductor gap than that for the helical coil configuration (figure 10), both antenna designs produced deeper heat penetration into tissue than was possible with thermal conduction heating alone. Additionally, the plane of the antenna gap was not the plane of optimum heat penetration for the HCS-10 antenna. Preliminary evidence indicated that radial profiles

obtained at various points along the helical coil were more reproducible, while heat penetration depths from the dipoles dropped off significantly with increasing axial distance in either direction from the antenna gap. This suggested a more cylindrical heating contour for the helical coil antennas than for the standard dipole antennas, although we were not able to quantify this with our percentage squareness parameter measured at the single distance of $r = 0{\cdot}5$ cm.

The exact mechanism of microwave radiation from the helical coil structure is not known. Although the coil is wound back along the feedline inner conductor, the helical coil antenna design may be considered as a variation of the omnidirectional or perpendicular mode helical radiator (Harris 1980). The antenna diameter is small compared to the wavelength, but significant magnetic flux linking the coil turns may produce an electric field which is predominantly circularly polarized about the coil. The specific polarization is dependent upon source frequency and load characteristics, and the length, diameter and spacing of the coil turns.

Further studies are necessary to characterize the performance of helical coil antennas using an increased coil length and/or lower source frequencies, and to determine the function of the outer conductor gap which distinguishes the HCC and HCS antenna configurations. It would be desirable to produce a discrete set of different heating length antennas for customized clinical treatment of variable-size tumours. Finally, proper spacing of multiple-antenna arrays for expanding the effective heating volume must be studied to ensure proper phase addition of the fields from the circularly polarized antennas.

In conclusion, it is anticipated that the helical coil antenna will simplify treatment planning considerations and perhaps increase the potential applications of interstitial microwave hyperthermia through improvements in the controllability, repeatability and localization of the heating field to a desired treatment volume at depth, regardless of location below the tissue surface.

Acknowledgements

We would like to thank Dr Ferdinand Volker at Lawrence Berkeley Laboratory for the use of an HP 8510 network analyser, Dr John R. Fike for a careful review of the manuscript, and Carol Shea for preparing this manuscript. This research was supported in part by NIH grants CA-39428 and CA-13525.

References

ASTRAHAN, M. A., and NORMAN, A., 1982, A localized current field hyperthermia system for use with 192-iridium interstitial implants. *Medical Physics*, **9,** 419–424.

BREZOVICH, I. A., ATKINSON, W. J., and LILLY, M. B., 1984, Local hyperthermia with interstitial techniques. *Cancer Research* (Suppl.), **44,** 4752s–4756s.

CHOU, C., CHEN, C., GUY, A., and LUK, K. K., 1984, Formulas for preparing phantom muscle tissue at various radiofrequencies. *Bioelectromagnetics*, **5,** 435–441.

DE SIEYES, D. C., DOUPLE, E. B., STROHBEHN, J. W., and TREMBLY, B. S., 1981, Some aspects of optimization of an invasive microwave antenna for local hyperthermia treatment of cancer. *Medical Physics*, **8,** 174–183.

DEWEY, W. C., 1984, Interaction of heat with radiation and chemotherapy. *Cancer Research* (Suppl.), **44,** 4714 s–4720 s.

EMAMI, B., and PEREZ, C. A., 1985, Interstitial thermoradiotherapy; an overview. *Endocurie. Hyperthermia, Oncology*, **1,** 35–40.

GUTIN, P. H., PHILLIPS, T. L., WARA, R. A., LEIBEL, S. A., HOSOBUCHI, T., LEVIN, V. A., and LAMB, B. S., 1984, Brachytherapy of recurrent malignant brain tumors with removable high-activity iodine–125 sources. *Journal of Neurosurgery*, **60,** 61–68.

HAHN, G. M., 1979, Potential for therapy of drugs and hyperthermia. *Cancer Research*, **39,** 2264–2268.

HALL, E. J., 1985, The biological basis for endocurietherapy. Endocurie. *Hypothermia and Oncology*, **1**, 141–152.

HARRIS, E. F., 1980, Helical antennas. *Antenna Engineering Handbook*, edited by Henry Jasik (San Francisco: McGraw-Hill), Chapter 7.

KING, R. W., TREMBLY, B. S., and STROHBEHN, J. W., 1983, The electromagnetic field of an insulated antenna in a conducting or dielectric medium. *IEEE Transactions, MTT*, **31**, 574–583.

LYONS, B. E., BRITT, R. H., and STROHBEHN, J. W., 1984, Localized hyperthermia in the treatment of malignant brain tumors using an interstitial microwave antenna array. *IEEE Transactions, BME*, **31**, 53–62.

MECHLING, J. A., and STROHBEHN, J. W., 1986, A theoretical comparison of the temperature distribution produced by three interstitial hyperthermia systems. *International Journal of Radiation, Oncology, Biology and Physics*, **12**, 2137–2149.

MOORTHY, C. R., HAHN, E. W., KIM, J. H., FRINGOLD, S. M., ALFIERI, A. A., and HILARIS, B. S., 1984, Improved response of a murine fibrosarcoma (METH-A) to interstitial radiation when combined with hyperthermia. *International Journal of Radiation, Oncology, Biology and Physics*, **10**, 2145–2148.

NEYZARI, A., and CHEUNG, A. Y., 1985, A review of brachyhyperthermia approaches for the treatment of cancer. *Endocurie. Hypertherm. Oncol.*, **1**, 257–264, 1985.

PEREZ, A., and EMAMI, B., 1985, A review of current clinical experience with irradiation and hyperthermia. *Endocurie. Hypertherm. Oncol.*, **1**, 265–277.

ROBERTS, D. W., COUGHLIN, C. T., WONG, T. Z., FRATKIN, J. D., Douple, E. B., and STROHBEHN, J. W., 1986, Interstitial hyperthermia and iridium brachytherapy in treatment of malignant glioma: a phase I clinical trial. *Journal of Neurosurgery*, **64**, 581–587.

SALCMAN, M., and SAMARAS, G. M., 1981, Hyperthermia for brain tumors: biophysical rationale. *Neurosurgery*, **9**, 327–335.

SAMARAS, G. M., 1984, Intracranial microwave hyperthermia: heat induction and temperature control. *IEEE Transactions, BME*, **31**, 63–69.

SNEED, P. K., MATSUMOTO, K., STAUFFER, P. R., FIKE, J. R., SMITH, V., and GUTIN, P. H., 1986, Interstitial microwave hyperthermia in a canine brain model. *International Journal of Radiation, Oncology, Biology and Physics*, **12**, 1887–1897.

STAUFFER, P. R., CETAS, T. C., and JONES, R. C., 1984 a, Magnetic induction heating of ferromagnetic implants for inducing localized hyperthermia in deep seated tumors. *IEEE Transactions, BME*, **31**(2), 235–251.

STAUFFER, P. R., CETAS, T. C., FLETCHER, A. M., DEYOUNG, D. W., DEWHIRST, M. W., OLESON, J. R., and ROEMER, R. B., 1984 b, Observations on the use of ferromagnetic implants for inducing hyperthermia. *IEEE Transactions, BME*, **31**(1), 76–91, 1984 b.

STAUFFER, P. R., SUEN, S., SATOH, T., and FIKE, J. R., 1986, Comparative thermal dosimetry of interstitial RF and microwave heating. pp. 1458–1462, *Proceedings of the IEEE Medical Biology Society Meeting*, Ft. Worth TX, November.

STROHBEHN, J. W., BOWERS, E., WALSH, J., and DOUPLE, D. B., 1979, An invasive microwave antenna for locally induced hyperthermia for cancer therapy. *Journal of Microwave Power*, **14**, 181–186.

TAYLOR, L. S., 1978, Electromagnetic syringe. *IEEE Transactions, BME*, **25**, 303–304, 1978.

TREMBLY, B. S., 1985, The effects of driving frequency and antenna length on power deposition within a microwave antenna array used for hyperthermia. *IEEE Transactions, BME*, **32**, 152–157.

VORA, N., FORELL, B., JOSEPH, C., LIPSETT, J., and ARCHAMBEAU, J. O., 1982, Interstitial implant with interstitial hyperthermia. *Cancer*, **50**, 2518–2523.

WINTER, A., LAING, J., PAGLIONE, R., and STERZER, F., 1985, Microwave hyperthermia for brain tumors. *Neurosurgery*, **17**, 1387–1399.